



HAL
open science

On experimental sensitivity analysis of an axisymmetric turbulent wake

M Grandemange, M Gohlke, V Parezanović, Olivier Cadot

► **To cite this version:**

M Grandemange, M Gohlke, V Parezanović, Olivier Cadot. On experimental sensitivity analysis of an axisymmetric turbulent wake. *Physics of Fluids*, 2012, 24, pp.035106. hal-01289900

HAL Id: hal-01289900

<https://ensta-paris.hal.science/hal-01289900>

Submitted on 17 Mar 2016

HAL is a multi-disciplinary open access archive for the deposit and dissemination of scientific research documents, whether they are published or not. The documents may come from teaching and research institutions in France or abroad, or from public or private research centers.

L'archive ouverte pluridisciplinaire **HAL**, est destinée au dépôt et à la diffusion de documents scientifiques de niveau recherche, publiés ou non, émanant des établissements d'enseignement et de recherche français ou étrangers, des laboratoires publics ou privés.

On experimental sensitivity analysis of an axisymmetric turbulent wake

M. Grandemange,^{1,2} M. Gohlke,² V. Parezanović,¹ and O. Cadot¹

¹*Unité de Mécanique, Ecole Nationale Supérieure de Techniques Avancées,
ParisTech, Chemin de la Hunière, 91761 Palaiseau Cedex, France*

²*PSA Peugeot Citroën, Centre Technique de Velizy,
Route de Gisy, 78943 Vélizy-Villacoublay Cedex, France*

The sensitivity to local disturbances of the turbulent wake over a 3D blunt body with an axisymmetric detachment is investigated at $Re = 2.1 \cdot 10^4$. The flow presents a favored $m = 2$ azimuthal symmetry set by two wings. The instantaneous wake is measured either above or below the plane containing the wings but leads a statistical symmetric wake. Topology shifts are random but occur mostly after a large number of global mode periods. The statistical symmetry is highly sensitive to any asymmetric disturbance. As a consequence, depending on its position a small control cylinder in the close wake fixes the wake to one asymmetric topology affecting shedding activity and drag. The effect of an axisymmetric perturbation ($m = 0$) on flow topology and dynamics is also studied ; it induces significant drag reductions and global mode modifications when acting on mixing layers. Whatever the disturbance, the sensitivity of the wake seems concentrated into the mixing layers and may depend more on their local turbulent characteristics than on the inviscid dynamics of vorticity.

I. INTRODUCTION

New theoretical efforts have allowed to obtain the structural sensitivity of global mode wakes in laminar regimes¹⁻³. Over bidimensional geometries, this approach is able to recover qualitatively the sensitivity obtained experimentally by Strykowski and Sceenivasan⁴. Recently, Meliga *et al.*^{5,6} performed similar studies in the wake of axisymmetric bodies ; zones of high sensitivity have been found in the recirculating bubble, particularly around the separatrix. Although the theory is still limited to basic flows and laminar regimes, this approach might provide a useful tool in the frame work of control strategy since it predicts the placement of a disturbance to efficiently affect global properties of the flow. For practical and industrial interests, the method should be extended to large Reynolds number flows over complex geometries. So far, no theory is available in turbulent regimes however, over cylinders, some qualitative similitudes persist between laminar theoretical analyses and experiments at moderate Reynolds numbers⁷⁻⁹. The empirical results of Parezanović and Cadot⁹ point out that the disturbance of the close wake leads to variations of global mode

$A = \langle a \rangle$	average value of a
$Std(a)$	standard deviation of a
a^*	non-dimensional value of a
$ \vec{a} $	modulus of a
c_D	drag coefficient
c_p	pressure coefficient
D	diameter of the body base
d_R	diameter of the control ring
$H = \delta_*/\theta$	boundary layer shape factor
L_b	recirculation length
p_0	inlet flow pressure
$P(\#A)$	probability of state $\#A$
$P(\#A \#B)$	probability of state $\#A$, given $\#B$
$Re = U_0 D/\nu$	Reynolds number
$St = fD/U_0$	Stouhal number
St_S	Strouhal number of the global mode
St_b	characteristic Stouhal number of the recirculation
T_b	characteristic time of the recirculation
$\vec{u} = u_x \cdot \vec{e}_x + u_y \cdot \vec{e}_y + u_z \cdot \vec{e}_z$	velocity
$u_{ij} = \sqrt{u_i^2 + u_j^2}$	modulus of velocity in plane (\vec{e}_i, \vec{e}_j)
U_0	inlet flow velocity
v_E	characteristic velocity of flow incorporation into the mixing layers
x_C	position x of the control cylinder
x_R	position x of the control ring
y_C	position y of the control cylinder
y_α	position y verifying $U_x^*(x^*, y^*, z^* = 0) = \alpha$
δ_{99}	boundary layer thickness based on 99% of freestream velocity
δ_*	boundary layer displacement thickness
δ_M	mixing layer thickness base on 10% and 90% of freestream velocity
Ω_z	mean vorticity in z direction
ρ	density of the fluid
θ	boundary layer momentum thickness

Table I: Nomenclature

frequency and base pressure. The associated physical mechanisms seem relied on the perturbation ability to change the size of the formation region of the von-Kármán street vortices and to interact

with the shear layers.

Over axisymmetric bodies, the dynamic of the separated flow is more complicated than the bidimensional von-Kármán street. Indeed, the wake undergoes several transitions associated to different wake regimes as the Reynolds number increases¹⁰. At very low Reynolds numbers, the flow is steady and axisymmetric. A first bifurcation is reported (for $Re \approx 210$ over spheres) : a steady azimuthal mode $m = 1$ appears. A lift force is generated and a pair of counter-rotating vortices develops downstream moving the wake off streamwise axis so the flow loses its axisymmetry but keeps a planar symmetry. A second bifurcation occurs at a higher Reynolds number ($Re \approx 277$ over spheres) : the wake starts oscillating but preserves the same planar symmetry. Becoming turbulent, the preference toward this azimuthal plane of symmetry vanishes and the flow becomes statistically axisymmetric¹¹. At moderate Reynolds numbers, the high frequency mixing layer instabilities in the close wake degenerate into large scale vortex loops developing from the end of the recirculation bubble ; the wake oscillates randomly^{10,12} and may get a helical structure highly coherent in space¹³⁻¹⁵. This unsteady global mode (dominant mode $m = 1$) is reported at $0.1 < St < 0.2$ depending on geometry and Reynolds number.

Previous experiments of passive and active control of the turbulent wake show connections between parameters of the control set-up, drag and global mode intensity^{14,16-20}. In particular, Berger *et al.*¹⁴ proves that disk forced to oscillate near the helical mode frequency stabilizes this mode in space and time at a coherence level close to 1. Weickgenannt *et al.*¹⁷ performed experiments displacing a control disk in the recirculation bubble pointing out different flow regimes depending on the disk position associated to important evolutions of drag and Strouhal number. However this control set-up may be too intrusive to be considered as a local perturbation.

The present work explores the sensitivity of wake of a 3D blunt body with a fixed axisymmetric flow separation at $Re = 2.1 \cdot 10^4$. Experiments of passive control using reasonably small devices are performed to disturb the flow with $m = 0$ and $m = 1$ perturbations ; to our knowledge, such an approach has not been carried out over bodies of revolution so far. The impact of the control device is reported through sensitivity maps of global mode frequency, pressure distribution on the body and estimation of the drag.

The article is organized as follows. First, the natural flow is analysed ; it is proved that two antisymmetric flows cohabit and generate a statistically symmetric natural flow. Then the sensitivity to different local perturbations is investigated. Any $m = 1$ disturbance change the statistical equilibrium of the mean flow moving it off axis. On the contrary, a $m = 0$ disturbance preserve the mean flow symmetry but has significant impacts global mode frequency and drag. The

sensitivity of the flow seems concentrated in the close wake, particularly into the mixing layers. Eventually, the effects of these disturbances on the wake orientation and global mode frequency are discussed ; past tridimensional bodies, the turbulent characteristic of the wake might play a greater role than the inviscid dynamics of vorticity.

II. EXPERIMENTAL SET-UP

The Eiffel type wind tunnel is an open loop air flow facility. The turbulent intensity is less than 0.3% and the homogeneity of the velocity over the 400 mm \times 400 mm blowing section is 0.4%. The wake is generated by a 3D symmetric blunt body ; its geometry is based on the "D" shape cylinder used in the experiments of Parezanović and Cadot⁸. The body is made up by a cylinder of diameter $D = 50$ mm and a half sphere forebody. The total length is $L = 125$ mm. The axisymmetric body is supported by two NACA 0021 profiles fixing the azimuthal planes of symmetry (xOy) and (xOz) (see Fig. 1). Most experiment are performed with the blunt body aligned to incoming flow, however when specified a small pitching angle ϵ is set to add an antisymmetric disturbance.

The main flow velocity is $U_0 = 6.5 \text{ m.s}^{-1}$ and the Reynolds number ($\text{Re} = U_0 D / \nu$) is $2.1 \cdot 10^4$. The velocities are defined as $\vec{u} = u_x \cdot \vec{e}_x + u_y \cdot \vec{e}_y + u_z \cdot \vec{e}_z$; $u_{ij} = \sqrt{u_i^2 + u_j^2}$ is the amplitude of velocity at the considered point in the plane (\vec{e}_i, \vec{e}_j). A and $Std(a)$ are respectively average value and standard deviation of any quantity a . The diameter D , density ρ , inlet velocity U_0 and static pressure p_0 are used to obtain non-dimensional values marked with an asterisk.

The separated flow is first controlled by a 3 mm diameter cylinder oriented along z direction and moved in the wake using a robot. x_C and y_C refer to the cylinder position (see Fig. 1(a)). Except when located on the streamwise axis, the cylinder is considered a $m = 1$ disturbance. The other control devices are flat rings with a length of 6 mm and a thickness of 1 mm mounted on a 3 mm diameter rod (see Fig. 1(b)). x_R represents the gap between the base of the body and the ring center. The point R remains on the streamwise axis so the symmetry of the body is preserved and the rings are associated to $m = 0$ perturbations. Nine ring diameters d_R between 0.7 and 1.1 D are used to disturb the close wake.

A wake analysis is made from PIV and stereo PIV measurements respectively in planes $z^* = 0$ and $x^* = 1.2$. Statistics from 2000 instantaneous velocity field estimate the fluctuating velocity energy. To get unsteady characteristics of the flow, a 1D hot wire probe mounted on a three-axis robot records the velocity in the wake at a sampling frequency of 2 kHz. Power spectra are then

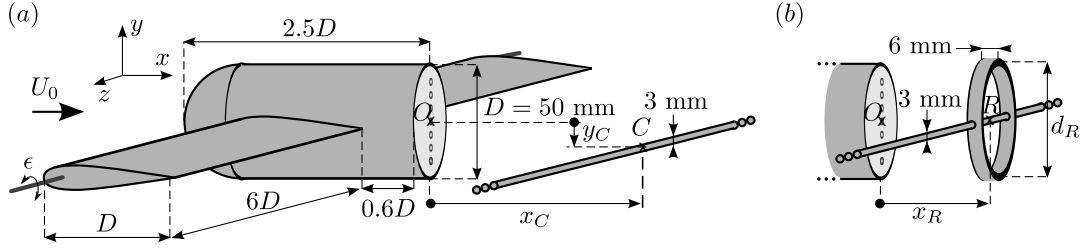


Figure 1: Experimental set-up of the body controlled by a 3 mm cylinder (a) and rings (b) ; O sets the origin of the coordinate system ; pitching angle $\epsilon = 0$ in most experiments.

calculated up to 1 kHz with a resolution of 0.5 Hz.

In addition, the pressure on the body is measured in the plane $z^* = 0$. Thirteen taps are located on the half sphere of the forebody every 15° ; the seven others give the pressure distribution on the base, the space between base taps is 6 mm. Pressure measurements are performed at 1 Hz over 120 s ; the sampling frequency of 1 Hz is limited by the acquisition device : the record is a mean over at least 1 s to preserve precision.

The drag is estimated by integration of the interpolated pressure on the surface projected on x direction ; pressure distributions in each region $y^* > 0$ and $y^* < 0$ are assumed axisymmetric :

$$\begin{aligned}
 C_D &= \frac{1}{\frac{1}{2}\rho\pi\frac{D^2}{4}V_0^2} \left[\iint_{body} p \, d\vec{s} \right] \cdot \vec{e}_x \\
 &\approx 4 \int_{y^*=-0.5}^{0.5} C_{pnose}(y^*) \cdot |y^*| \, dy^* \\
 &\quad - 4 \int_{y^*=-0.5}^{0.5} C_{pbase}(y^*) \cdot |y^*| \, dy^*.
 \end{aligned} \tag{1}$$

For the uncontrolled flow, the so-evaluated drag is $C_{D0} = 0.261 \pm 0.002$. Experimenting the method presented by Weickgenannt *et al.*¹⁷ based on momentum deficiency in the far wake, a higher value of 0.29 is measured, partially due to friction effects. When the control device is in the wake, its contribution to the drag is neglected.

III. RESULTS

A. Natural flow

The boundary layer at the trailing edge is fully turbulent and depends on the azimuth due to the presence of the wings in the plane $y^* = 0$. The boundary layers at detachment in planes $y^* = 0$ and $z^* = 0$ are presented on Figure 2(a). A separation is observed on the upper and lower part of the the end of the forebody. The flow reattaches turbulent on the cylindrical part before the massive separation at the trailing edge. This boundary layer history leads to the mean and fluctuating velocity profiles in the plane $z^* = 0$ (see empty and filled circles on Fig. 2(a)). The energy of the fluctuations of velocity diminishes when y^* increases and tends to the free flow level of turbulence. This particularly high fluctuation level in the entire boundary layer is a result of the forebody detachment.

In the plane $y^* = 0$, the wake of the wings leads to a velocity deficiency and a turbulent boundary layer at the trailing edge at $y^* \approx 0$ (see empty and filled squares on Fig. 2(a)). As the wake of the wings is present at $y^* = 0$, the fluctuations of velocity remains large even outside the boundary layer. The characteristics obtained from these velocity profiles are presented in table II. The high shape factor of the turbulent boundary layer is certainly due to the adverse pressure gradient along the side of the body.

	BL at $y^* = 0.5$ and $z^* = 0$	BL at $y^* = 0$ and $z^* = 0.5$
δ_{99}	1.57 mm ± 0.05 mm	1.82 mm ± 0.05 mm
δ_*	0.36 mm ± 0.02 mm	0.40 mm ± 0.02 mm
θ	0.18 mm ± 0.02 mm	0.19 mm ± 0.02 mm
H	2.0 ± 0.3	2.1 ± 0.3

Table II: Boundary layer characteristics at the trailing edge.

After detachment, the mixing layers grows from the trailing edge to the far wake. Figure 2(b) displays the streamwise velocity profiles in plane $z^* = 0$ at different positions x^* . The size of the mixing layer is defined as $\delta_M(x) = y_{0.9}(x) - y_{0.1}(x)$ with $y_\alpha(x)$ verifying $U_x^*(x, y_\alpha(x)) = \alpha$. The experiments of Champagne *et al.*²¹ report that plane turbulent mixing layers has a characteristic growth rate constant $d\delta_M^*/dx^* \sim 0.1$. In parallel, the eddy viscosity model predicts that it expands toward the low velocity domain²². The contours of $U_x^* = 0.1, 0.5$ and 0.9 (positions of $y_\alpha(x)$ for

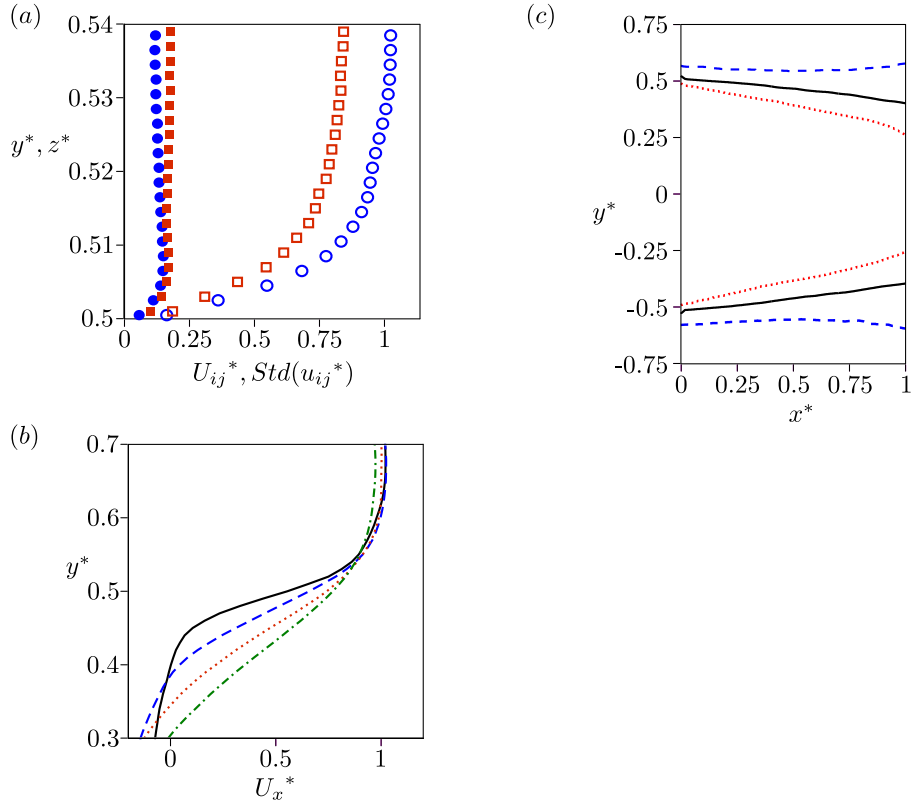


Figure 2: (a) Mean and fluctuating velocity profiles respectively empty and filled markers at the trailing edge in plane $z^* = 0$ (blue \circ) and $y^* = 0$ (red \square); the hot wire probe measures respectively U_{xy} and U_{xz} . (b) Streamwise velocity profiles in the upper mixing layer from PIV in plane $z^* = 0$ at different x^* positions: —, $x^* = 0.2$; --, $x^* = 0.4$; ··, $x^* = 0.6$; -·-, $x^* = 0.8$. (c) Contours of streamwise velocity U_x^* from PIV in plane $z^* = 0$: ··, 0.1; —, 0.5; --, 0.9.

$\alpha = 0.1, 0.5$ and 0.9) are plot on Figure 2(c). The growth of δ_M is approximately linear between $x^* = 0.1$ and $x^* = 0.7$ and $d\delta_M^*/dx^*$ is measured respectively at 0.17 and 0.18 for the upper and lower mixing layer. The expansion occurs toward the recirculation bubble where $U_x^* \sim 0$, the contours $U_x^* = 0.9$ being roughly parallel to the streamwise axis. This particularly high growth rate in comparison to the results presented by of Champagne *et al.*²¹ may be due to the axisymmetry of the wake but also to the oscillations induced by the presence of a global mode. Indeed, the power spectrum analysis of hot wire probe signals at $(x^*, y^*, z^*) = (4, 0.5, 0)$ reports a wake oscillation at frequency $f_S = 25.8$ Hz, *i.e.* $St_S = 0.199$ (see Fig. 3). The two peaks at $St \approx 0.05$ and 0.07 correspond to wind tunnel signature.

Figure 4(a) displays the streamlines of the time-averaged PIV measurements in the plane

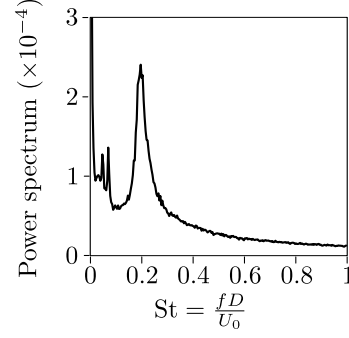


Figure 3: Power spectrum analysis of hot wire probe signal at $(x^*, y^*, z^*) = (4, 0.5, 0)$.

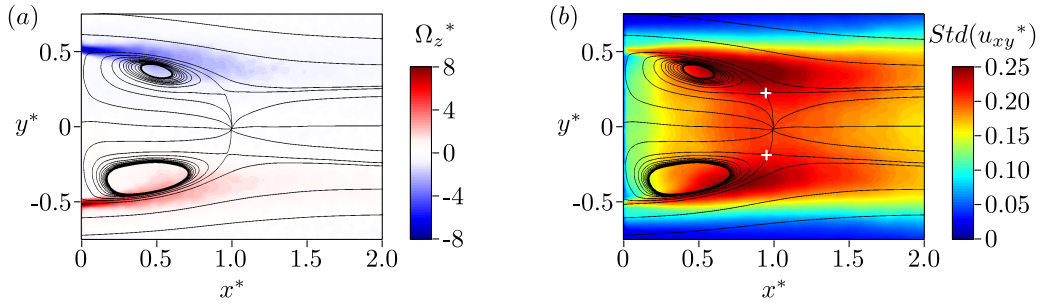


Figure 4: Streamlines of the time-average vector field in the plane $z^* = 0$; colormap of the mean vorticity Ω_z (a) and fluctuating velocities (b) ; white cross, collar point.

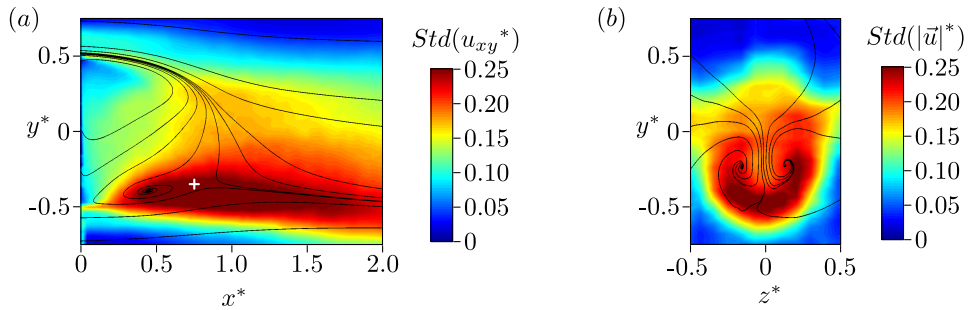


Figure 5: Streamlines of the velocity field in the plane $z^* = 0$ (a) and in the plane $x^* = 1.2$ (b) for slightly nose-up configuration, state #1 ; colormap of the fluctuating velocities ; white cross, collar point.

$z^* = 0$. The natural wake is symmetric referring to the plane $y^* = 0$ with two recirculation structures and two collar points at $x^* = 0.95$ and $y^* \approx \pm 0.2$ (see Fig. 4(b)). This topology is consistent with the two pairs of counter-rotating vortex proposed by Delery²³ ; the converging streamlines at $y^* \approx \pm 0.2$ for $x^* > 1$ are the signatures of these streamwise vortices in the symmetry plane $z^* = 0$, one pair at $y^* \approx 0.2$ and the other at $y^* \approx -0.2$. The vorticity concentrated in the

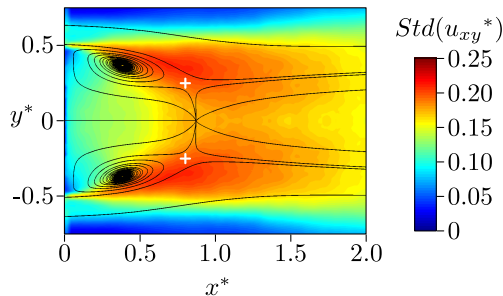


Figure 6: Flow computed from velocity field #1 in plane $z^* = 0$ (see Fig. 5(a)) and the expected velocity field for state #2.

boundary layer vanishes from the detachment to the end of the recirculating bubble. The vorticity is only measured near the recirculation separatrix : the recirculation structures do not contain vorticity. The maximum fluctuating energy is measured at $y^* \approx \pm 0.4$ and $x^* \approx 0.8$ (see Fig. 4(b)). These fluctuations are partially associated to the development of the unsteady global mode. As expected, it is equally present at the top and the bottom of the end of the recirculation bubble. In agreement with remarks present in literature^{17,23}, the symmetry of the wake is highly sensitive to the set-up configuration. An ϵ incidence moves the whole wake up or down. Figures 5(a)–(b) present the asymmetric wake topology for a slightly nose-up configuration. Measurements in the plane $x^* = 1.2$ show only one pair of counter-rotating vortices at $y^* \approx -0.3$ and $z^* \approx \pm 0.2$ just above a single zone of intense fluctuations. Therefore, as soon as the symmetry is lost, the unsteady $m = 1$ mode develops mostly from the lower part of the wake. It is associated to the formation of parallel hairpin shaped vortex loops at the end of the recirculation bubble^{10,24}. When the symmetry is preserved, these vortex loops must develop statistically from both sides of the wake.

The observed balanced wake for $\epsilon = 0$ (see Fig. 2(b)) is consistent with an average of two asymmetric topologies (named #1 and #2), each of them being respectively close to the flow presented on Figures 5(a)–(b) and its symmetric referring to the plane $y^* = 0$. Indeed, averaging the velocity field \vec{U}_ϵ for state #1 shown on Figure 5(a) with the expected flow for state #2, an artificial velocity field can be computed: $U_x(x^*, y^*) = \frac{1}{2}(U_{x\epsilon}(x^*, y^*) + U_{x\epsilon}(x^*, -y^*))$ and $U_y(x^*, y^*) = \frac{1}{2}(U_{y\epsilon}(x^*, y^*) - U_{y\epsilon}(x^*, -y^*))$. This artificial wake presented on Figure 6 has exactly the same properties as the measured one over a lined-up body : two collar points associated to two zones of intense fluctuations of velocity at $y^* \approx \pm 0.4$.

Two different wake positions are then expected for the flow over a lined-up configuration *i.e.* $\epsilon = 0$. When the wake follows the configuration #1, the upper recirculation structure is bigger and closer to the base than the lower one. This asymmetry of the recirculation bubble leads to an average diagonal recirculating flow and a non-uniform pressure distribution on the base ; the base pressure gradient dC_p/dy^* is negative in state #1 (see Fig 7(a)). The slope of the linear fit of the base pressure distribution gives the average pressure gradient and indicates whether the instantaneous flow follows the state #1 or #2. Hence, each record of base pressure distribution gives the dominant topology over the second of measurement.

The time evolution of the base pressure signal during $5 \cdot 10^3$ s is studied. The pressure gradient, *i.e.* the dominant topology, is shown on Figure 7(b) over 1000 s . Two preferred positions are visible at $dC_p/dy^* \approx \pm 0.1$. This point is confirmed by the probability density function presented on Figure 7(c). The two topologies #1 and #2 respectively associated to negative and positive gradients (-0.7 and 0.9) are clearly visible. The presence of the minimum between these peaks suggests that a sampling period of 1 s remains below the mean shift time estimated at 4.6 s, *i.e.* more than 100 global mode periods. The standard deviation of the base pressure gradient is 0.084. This value is equivalent to the absolute values of pressure gradients associated to states #1 and #2 presented on the histogram Figure 7(b). Such a high value is then an indicator of the coexistence of the two wake topologies. Eventually, the spectrum analysis of this signal over the $5 \cdot 10^3$ s does not present any characteristic frequency : the process seems random.

The two asymmetric topologies are then discriminated against the sign of the base pressure gradient. The probability of state #1 or #2 at a moment t (resp. named $S_t = \#1$ and $S_t = \#2$) depends not only on geometrical parameters like incidence but also on the past events (see Tab. III). $P(S_t = \#1) < P(S_t = \#1 | S_{t-1} = \#1) < P(S_t = \#1 | S_{t-1} = S_{t-2} = \#1)$ (idem for topology #2), $P(\#A|\#B)$ referring to the conditional probability of #A, given #B. As a result, a configuration is more likely to appear at t if it was already there the seconds before.

$P(S_t = \#1) = 0.53$	$P(S_t = \#2) = 0.47$
$P(S_t = \#1 S_{t-1} = \#1) = 0.79$	$P(S_t = \#2 S_{t-1} = \#2) = 0.77$
$P(S_t = \#1 S_{t-1} = S_{t-2} = \#1) = 0.85$	$P(S_t = \#2 S_{t-1} = S_{t-2} = \#2) = 0.80$

Table III: Probabilities of states #1 and #2 depending on the previous states over lined-up uncontrolled configuration (precision better than 0.02), $P(\#A|\#B)$ is the conditional probability of #A, given #B

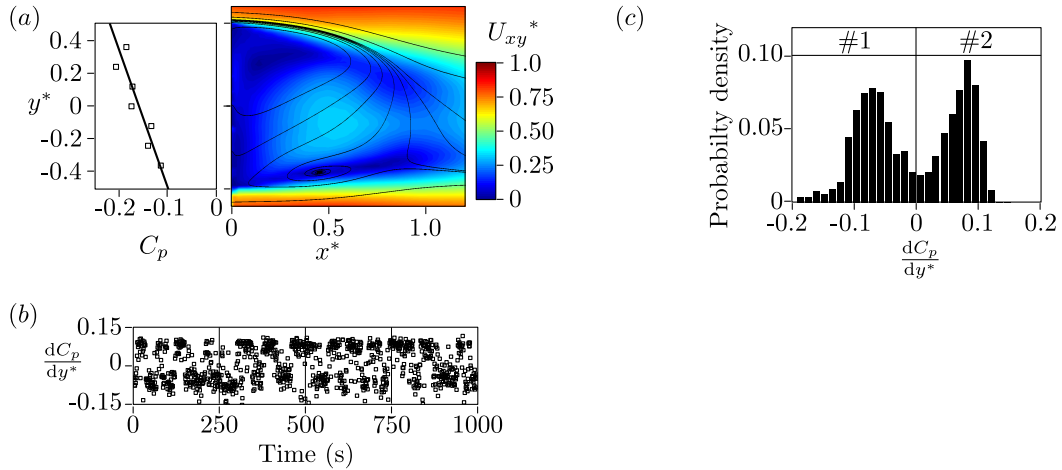


Figure 7: (a) Base pressure distribution of topology #1 characterized by the negative slope of the linear fit (continuous line), the corresponding bubble velocity field from Figure 4(b) is presented. (b) Time evolution of 1 s averaged base pressure gradient over 1000 s. (c) Probability density function of base pressure slope in y direction (precision ± 0.01).

B. 3 mm control cylinder in the wake

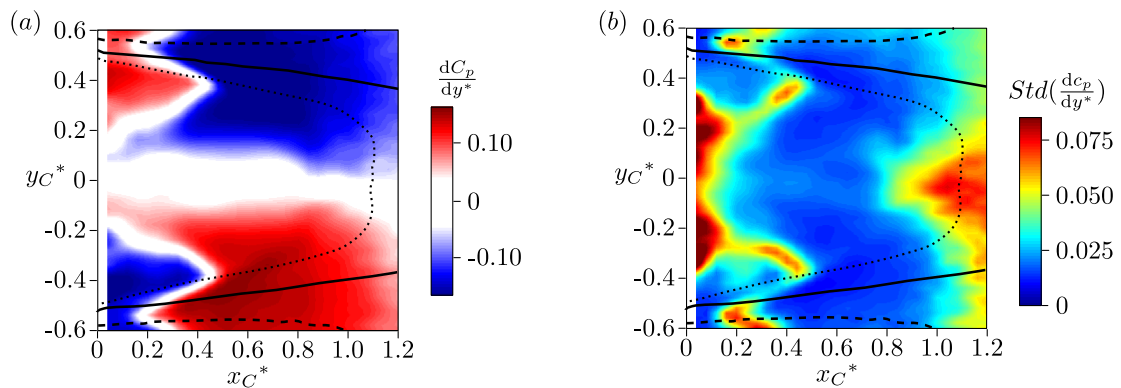


Figure 8: Effect of the position of the 3 mm control cylinder on dC_p/dy^* (a) and on $Std(dC_p/dy^*)$ (b); contours of U_x^* for the natural flow: \cdots , 0.1 ; $—$, 0.5 ; $- - -$, 0.9.

The asymmetric wake observed for a slight pitching angle highlights that average topology is sensitive to any tiny change in geometrical configuration. As a consequence the control cylinder which can be seen as a $m = 1$ steady disturbance should as well have significant impacts on the flow. The base pressure gradient (*i.e.* the dominant topology) obtained as a function of the cylinder position is presented on Figure 8(a). As expected, this $m = 1$ perturbation is highly

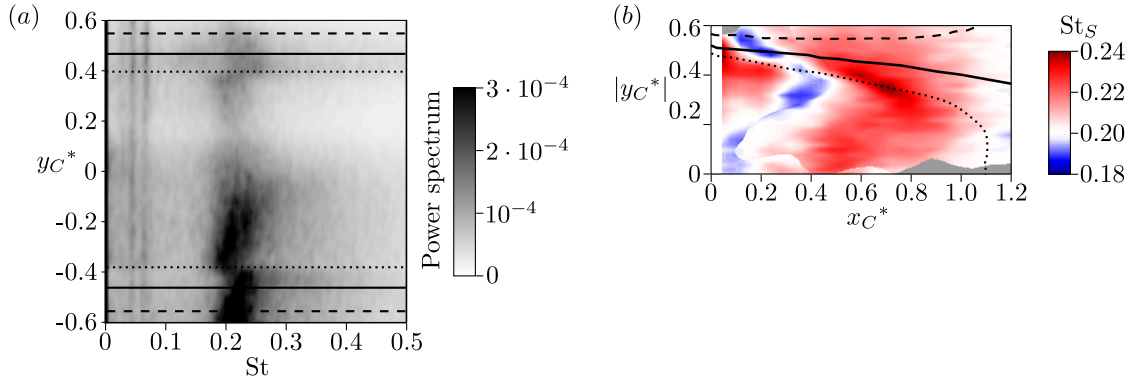


Figure 9: (a) Effect of the position of the control cylinder y_C^* at $x_C^* = 0.5$ on the power spectrum at $(x^*, y^*, z^*) = (4, 0.5, 0)$; positions of U_x^* for the natural flow: \cdots , 0.1; $—$, 0.5; $--$, 0.9. (b) Strouhal of the global mode as a function of the cylinder position; the grey areas correspond to the absence of peak in the measured power spectrum; contours of U_x^* of the natural flow: \cdots , 0.1; $—$, 0.5; $--$, 0.9.

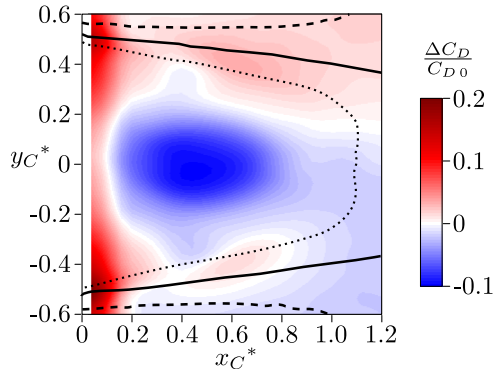


Figure 10: Effect of the position of the control cylinder on drag; contours of U_x^* for the natural flow: \cdots , 0.1; $—$, 0.5; $--$, 0.9.

efficient in selecting the state #1 or #2. When positioned at $x_C^* = 0.2$ and $y_C^* = -0.3$, it forces the topology #1 (see Fig. 11(a)); if moved further downstream at constant $y_C^* = -0.3$ then the configuration #2 dominates. When $y_C^* = 0$, the average wake is balanced (see Fig. 11(b)). For $x_C^* < 0.5$ and $y_C^* \neq 0$, there are also positions of the control cylinder where no pressure gradient is induced despite the asymmetry of the configuration. At these locations, the fluctuation levels of base pressure gradient over the 120 measurements is close to the natural value (see Fig. 8(b)). This points out that both topologies #1 and #2 are present in the wake, the shift characteristic time being implicitly between 1 s and 60 s. Further downstream, for $x_C^* > 1$, the flow is less influenced by the control cylinder: the effect of the disturbance is not important enough to really

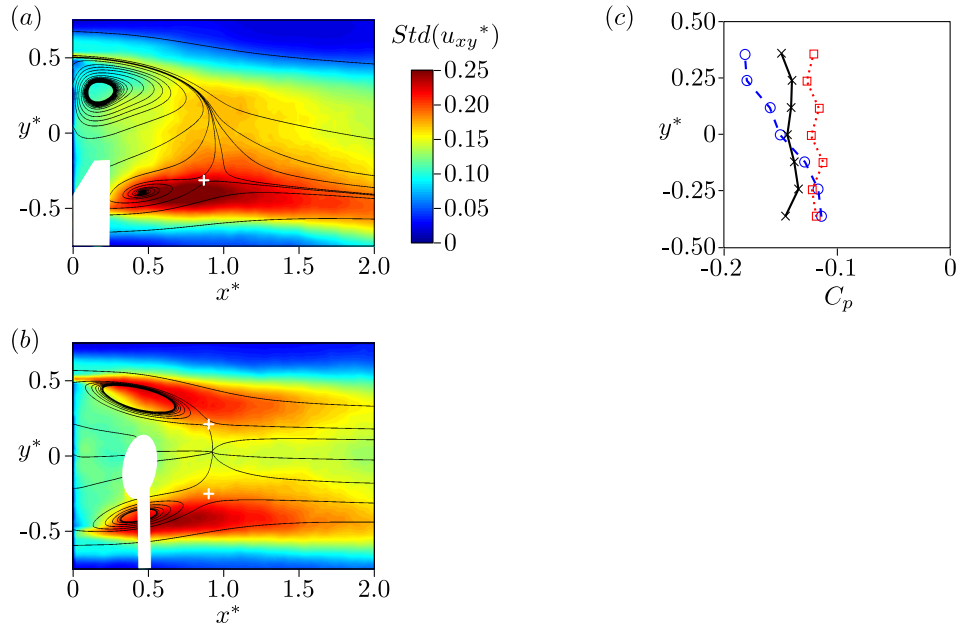


Figure 11: Streamlines in the plane $z^* = 0$ for the controlled case $x_C^* = 0.2$ and $y_C^* = -0.3$ (a) and $x_C^* = 0.5$ and $y_C^* = 0$ (b) ; colormap of the fluctuating velocities ; white cross, collar point. (c) Base pressure distribution: — (\times), natural flow ; -- (\circ), $x_C^* = 0.2$ and $y_C^* = -0.3$ (see Fig. 11(a)) ; \cdots (\square), $x_C^* = 0.5$ and $y_C^* = 0$ (see Fig. 11(b)).

set an asymmetric base pressure gradient and the fluctuation levels get back to the values of the uncontrolled case. On the contrary, wherever the cylinder induces high positive or negative base pressure gradient, *i.e.* topology #1 or #2, fluctuation levels of base pressure gradient are much lower than the natural value : the control cylinder tends to stabilize the wake in one asymmetric state depending on its position. Eventually, the fluctuations of base pressure remain quite low when placed in the middle of the recirculation bubble ; either the wake is stabilized in a topology with a uniform base pressure distribution or the mean shift time is under the measurement frequency of 1 Hz.

The cohabitation of the two topologies is then altered by this $m = 1$ disturbance and the dynamic of the global mode is equally affected. The spectrum analysis of the hot wire probe signal at $(x^*, y^*, z^*) = (4, 0.5, 0)$ is presented on Figure 9(a) as a function of the cylinder position y_C^* for $x_C^* = 0.5$. As the probe is at $y^* = 0.5$, the power spectrum map is not symmetric referring to $y_C^* = 0$. A higher level energy is measured on the entire power spectra when the flow follows topology #2, *i.e.* $y_C^* < 0$ at $x_C^* = 0.5$. Indeed, the fluctuations of velocity are mostly

concentrated at the upper part of the recirculation and are convected downstream to the hot wire probe whereas the levels of fluctuations are low at the probe while the flow follows state #1. Figure 9(b) report the global mode frequency at positions where a peak of energy is present in the power spectrum. This map is particularly correlated to the map of absolute values of base pressure gradient. The more the control cylinder induced an asymmetric topology, the higher the frequency is. On the contrary, St_S tends to be reduced where the control cylinder sets $dC_p/dy^* \sim 0$. An exception is observed when $y_C^* \approx 0$ but the energy associated to the global mode activity is spreading over a large band of frequency and St_S is poorly defined. For these positions, the total energy of the fluctuations of velocity may be slightly lower compared to that of the natural flow (compare Fig. 11(b) to Fig. 4(b)) but remains at the same order of magnitude. In addition, the two collar points are still observed in the wake. This tends to indicate that the flow is not stabilized but that the two states #1 and #2 may still be present with a shifting time smaller than 1 s.

In parallel to these different flow modifications, drag is estimated through the pressure distribution on the body. Drag reductions are mostly observed for $x_C^* \approx 0.5$ and $y_C^* \approx 0$ (see Fig. 10). The optimal position leads to a 8% decrease in drag mostly associated to a recovery of base pressure (see Fig. 11(c)) ; the forebody pressure distribution is found independent of the cylinder position. When the cylinder induces $dC_p/dy^* \approx 0$ for $y_C^* \neq 0$, there is almost no effect on the drag. At these locations, the flow does not seem disturbed by the cylinder, the only difference is that the global mode frequency is slightly reduced.

C. Rings acting on mixing layers

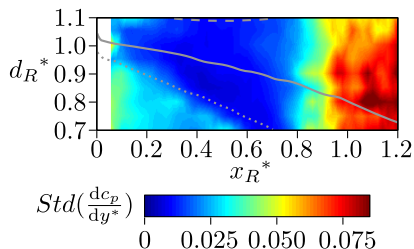


Figure 12: Effect of the position of the control rings on $Std(dC_p/dy^*)$; contours of U_x^* from uncontrolled flow are plot: \cdots , 0.1 ; $—$, 0.5 ; $--$, 0.9.

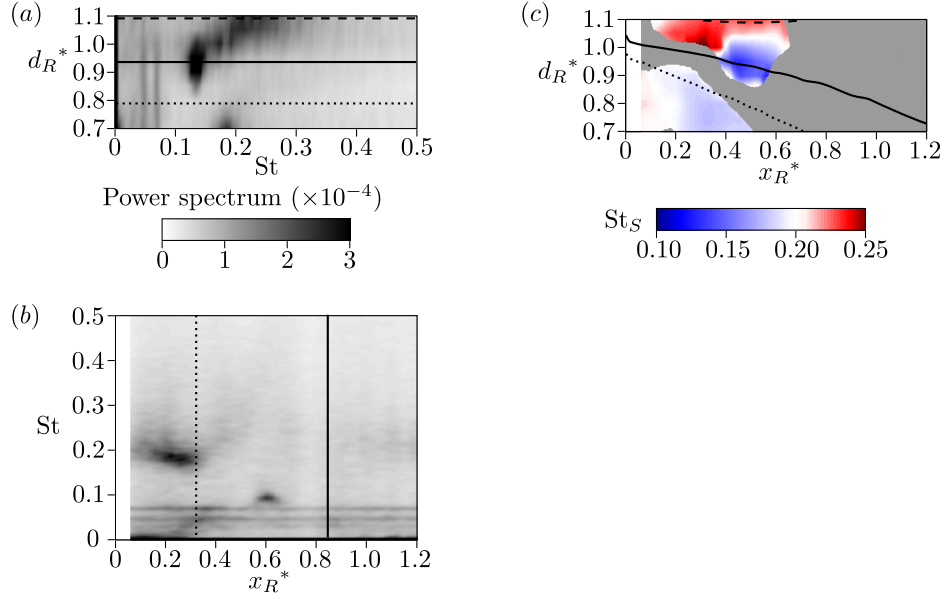


Figure 13: (a) Effect of the ring diameter d_R^* at $x_R^* = 0.5$ on the power spectrum at $(x^*, y^*, z^*) = (4, 0.5, 0)$ (see Fig 3 for comparison to natural flow) ; positions of U_x^* of the natural flow are plot: $\cdot\cdot$, 0.1 ; $—$, 0.5 ; $--$, 0.9.. (b) Effect of the position x_R^* of the $d_R^* = 0.85$ ring on the power spectrum at $(x^*, y^*, z^*) = (4, 0.5, 0)$ (see Fig. 3 for comparison to natural flow and Fig. 13(a) for legend). (c) Strouhal number of the global mode as a function of the ring position ; the grey areas correspond to the absence of peak in the measured power spectrum ; contours of U_x^* for the natural flow: $\cdot\cdot$, 0.1 ; $—$, 0.5 ; $--$, 0.9.

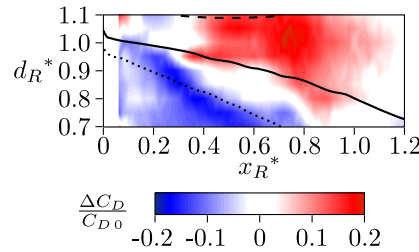


Figure 14: Effect of the position of the control ring on drag ; contours of U_x^* from uncontrolled flow are plot: $\cdot\cdot$, 0.1 ; $—$, 0.5 ; $--$, 0.9.

The sensitivity of the flow to $m = 0$ disturbances is now studied placing the rings in mixing layers. The contribution of the 3 mm support to the following results can be estimated through the effect of the control cylinder analyzed in the previous section when $y_C^* = 0$. As the perturbations introduced by the rings are symmetric, the base pressure gradient remains null but its fluctuation levels are still an indicator of stability. These fluctuations as a function of the ring diameter and position are presented on Figure 12. For $x_R^* < 0.8$ the fluctuations of base pressure gradient tend

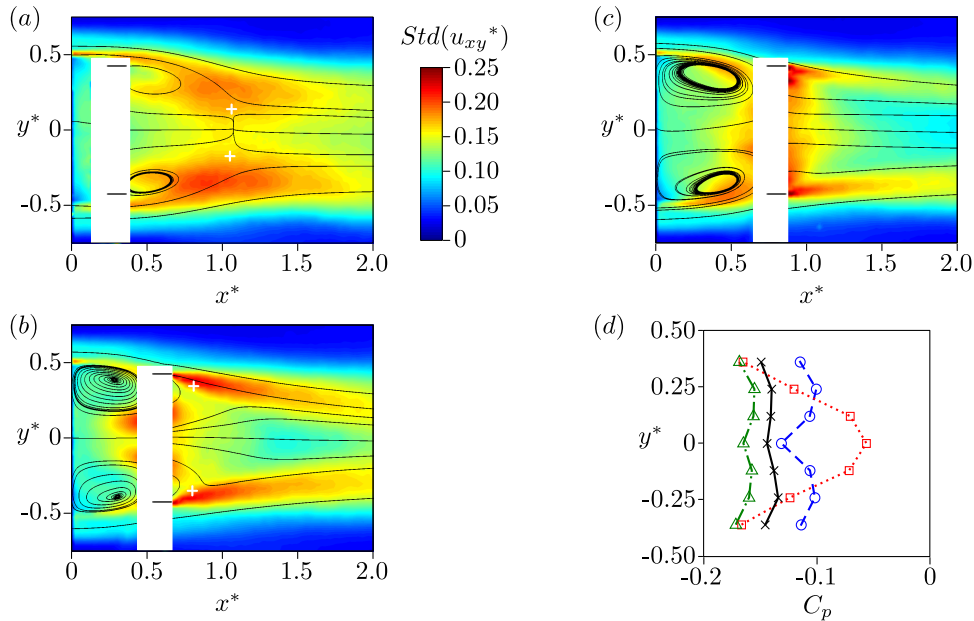


Figure 15: (a) Streamlines in the plane $z^* = 0$ for the controlled flow with the $d_R^* = 0.85$ diameter ring at $x_R^* = 0.3$; colormap of the fluctuating velocities ; white cross, collar point. (b) Idem Figure 15(a) at $x_R^* = 0.6$. (c) Idem Figure 15(a) at $x_R^* = 0.8$. (d) Base pressure distribution: — (×), natural flow ; -- (○), $x_R^* = 0.3$ and $d_R^* = 0.85$ (see Fig. 15(a)) ; ·· (□), $x_R^* = 0.6$ and $d_R^* = 0.85$ (see Fig. 15(b)) ; -·- (△), $x_R^* = 0.8$ and $d_R^* = 0.85$ (see Fig. 15(c)).

to be attenuated referring to the natural flow. In particular, the impact of the control ring on $Std(dc_p/dy^*)$ follows the inner frontier of the mixing layer. As for the control cylinder, these low values mean that either the wake is stabilized or the shift characteristic time is smaller than the measurement sampling frequency. For $x_R^* > 0.8$, the fluctuations of base pressure gradient return close to its natural values.

The modification of the global mode activity due to the presence the control rings is now considered. Figures 13(a)–(c) present the power spectrum of the hot wire probe signal at $(x^*, y^*, z^*) = (4, 0.5, 0)$. For small ring diameters in the close wake ($d_R^* < 0.85$ and $x_R^* < 0.2$), the disturbance is not in the mixing layer, the global mode frequency and amplitude are close to the natural case. As the disturbance reaches the inner part of the mixing layer for $x_C^* < 0.4$, the shedding frequency is decreased by approximately 15%. While the ring diameter increases, the perturbation affects the middle of the mixing layer and the global mode is reported far less energetic and then poorly defined (grey zones on Fig. 13(c)). Reaching the outer part of the mixing layer, the global mode is measured again but at a higher frequency in comparison to the natural

value.

Further downstream for $0.4 < x_C^* < 0.6$, a different scheme is observed (see Fig. 13(a)). As measured for $x_C^* < 0.4$, the global mode frequency is reduced for small ring diameters and the peak of energy in the spectra disappears increasing d_R^* . In the middle of the mixing layer, a new global mode regime is measured with a frequency of $St_S \approx 0.1$. Eventually, for $d_R^* > 1$, the perturbation of the outer part of the mixing layer leads to an increase in global mode frequency. For $x_R^* > 0.6$ whatever d_R^* is, there is no more peak reported in the power spectra. The attenuation of the global mode may be due to the presence of the 3 mm support. Indeed, Figure 9(b) points out that the control cylinder prevent the global mode development when placed on the streamwise axis for $x_C^* > 0.7$. Then, for these locations, the effect of the support may not be negligible.

These evolutions in the dynamic of the flow result in drag reductions and increases. Figure 14 presents the estimation of the drag depending on the ring diameter and position. Alike the global mode activity, the effect of the rings approximately follows the position of the mixing layer in the natural flow. The optimal drag reductions are observed when the control device acts on the inner part of the mixing layers. In opposition, drag is globally increased when the outer part of the mixing layer is disturbed. An exception is present for $x_C^* \approx 0.2$ where drag is also decreased for the highest ring diameters. Thus, the drag evolutions do not directly correspond to the global mode frequency map presented on Figure 13(c). Eventually, as observed with the control cylinder, if $x_R^* > 0.9$ the effect is limited on drag indicating that the sensitivity of the flow is concentrated particularly in the close wake mixing layers.

Different flow topologies correspond to these variations of drag and shedding frequency ; three of them are presented on Figures 15(a)–(c) corresponding to $x_R^* = 0.3, 0.6$ and 0.8 for $d_R^* = 0.85$. The associated spectra can be observed on Figure 13(b). At $x_R^* = 0.3$, a 14% decrease in C_D is measured. The associated velocity field is displayed on Figure 15(a). The recirculating structures move downstream in comparison to the original flow (see Fig. 3 for comparison) and the bubble length L_b is increased by 7.5%. The pressure recovery induced by the control device is distributed on the entire base area (see Fig. 15(d)). This position of the ring also corresponds to a slight reduction in global mode frequency is measured at $St = 0.17$ (see Fig. 13(b)).

Another topology is obtained with $x_R^* = 0.6$ and $d_R^* = 0.85$. PIV measurements presented on Figure 15(b) point out that the mixing layers reattach on the flat ring. The directions of the

streamlines around $x^* \approx 0.8$ indicate the presence of two stagnation points downstream the ring but after the recirculation bubble ; thus they may not be associated to equivalents of states #1 and #2 but rather to the proper wake of the ring. The area where $U_x^* < 0$ is strongly shortened and the recirculation centers move near the body and the curvature of the recirculation separatrix increases reducing peripheral base pressure. As shown on Figure 15(d), a compression occurs at the center of the body due to an intensified recirculating flow in average. However this high pressure at the base center is not sufficient to offset the loss of peripheral pressure. Indeed, the assumed axisymmetry of the base pressure implies that the area associated to the pressure considered to calculate drag is proportional to $|y^*|$ (see (1)). The base pressure at $y^* \approx 0$ has then a smaller impact on drag than at the periphery. The drag is measured equal to the uncontrolled case despite this different topology corresponding to the low frequency global mode ($St_S \approx 0.1$).

A third topology associated to high drag case is presented on Figure 15(c). Alike for $x_R^* = 0.6$, the flow reattaches on the rings and the recirculating structures are moved closer to the base of the body inducing a shorter recirculation length. The drag is increased due to the loss of pressure reported on the entire base : in opposition to the $x_R^* = 0.6$ there is not intense backward flow to counter the loss peripheral base pressure. This position of the ring is associated to an absence of global mode activity.

IV. DISCUSSION

A. On the global mode frequency

An unsteady global mode is usually observed in the flow past bluff bodies at moderate Reynolds numbers : its frequency and energy depend on different parameters. Over cylinders, Gerrard²⁵ presents a dynamic of the bubble in the wake considering the von-Kármán vortices. The flow entrained from the bubble to the mixing layers is renewed by the flow injected at the end of the recirculation through the velocity induced by the shear layers rollings. This model is highly related to the vorticity dynamic following Biot & Savart law and leads to a dependence between the characteristics of the shear layers and the global mode activity. The experiments of Parezanović and Cadot⁹ recently confirm that the disturbance of the distance between the two shear layers or their intensity impacts the global mode frequency. The presented results are in good agreement with this Gerrard's analysis : the Strouhal number of the global mode of the wake is governed by

the shear layer interaction.

The flow of over tridimensional geometries seems less influenced by the inviscid dynamics of the vorticity in the wake. The global mode does not correspond to intense shedding and the refill of the bubble presented by Gerrard is no more relevant. However, the dynamics of the flow can still be analyzed considering that the turbulence characteristic of the wake is dominant. The growth of the mixing layer is associated to the entrainment of fluid from both the bubble and the freestream flow at a characteristic velocity v_E following the relationship

$$v_E dx \sim U_0 [\delta_M(x + dx) - \delta_M(x)],$$

then

$$v_E^* \sim \frac{d\delta_M^*}{dx^*}.$$

Estimating the bubble shape area and volume roughly at $L_b D$ and $L_b D^2$ with L_b the length in x direction, a characteristic time of the dynamic of the bubble T_b can be defined. T_b corresponds to the time needed to empty the volume of the bubble with a outflow speed v_E over the interface.

$$L_b D v_E T_b \sim L_b D^2,$$

$$T_b \sim \frac{D}{U_0 v_E^*} \sim \frac{D}{U_0 \cdot d\delta_M^*/dx^*}.$$

The associated Strouhal number is

$$St_b \sim \frac{D}{U_0 T_b} \sim \frac{d\delta_M^*}{dx^*}. \quad (2)$$

If the turbulent characteristic of the flow dominates its vorticity dynamic, then the global mode frequency of the recirculation bubble may linearly depend on the growth of the mixing layers in turbulent flows. The value of $d\delta_M^*/dx^* \approx 0.17$ is measured in our experiments for the natural flow where the Strouhal of the shedding is measured at 0.199 so $St_b \approx \alpha d\delta_M^*/dx^*$ with $\alpha \approx 1$. This dependence is consistent with the observations of Achenbach²⁴ on the Strouhal number of the wake oscillation past a sphere. The frequency of this mode increases with the Reynolds number from $St = 0.12$ at $Re = 6 \cdot 10^4$ to $St = 0.20$ at $Re = 3 \cdot 10^5$ just before the critical Reynolds number is reached. At moderate Reynolds number, the mixing layer is laminar in the close wake and its growth is slow ; this state is then associated to a low mode frequency. As the Reynolds number

increases, the mixing layer turns into turbulence before the end of the recirculation. The higher the Reynolds number is, the sooner the transition occurs. This results in an increasing flow entrainment into the mixing layers and an higher global mode frequency.

The effect of the control ring on the shedding frequency may be interpreted with this basic model (see Fig. 13(c)). When the ring disturb the inner part of the mixing layer, the fluctuations of velocity are reduced in the mixing layers. Their growth rate is then attenuated corresponding to an increase in the recirculation length (see Fig. 14(a)). The associated shedding frequency is measured slightly reduced. When the rings act on the outer mixing layer in the close wake, the mixing layer may become more unstable and enhance fluid entrainment increasing the Strouhal number of the mode.

Further downstream, a part of the mixing layer flow is oriented toward the streamwise axis and the rings have their own wake. Thus, the dynamic of the flow changes drastically and the mode frequency at $St \approx 0.1$, when observed, cannot be compared to the natural value. Eventually, the influence of the control cylinder on the global mode frequency is not discussed here. Indeed, $m = 1$ perturbations mostly impact the planar symmetry and the orientation of the wake, these effects are analyzed in the following section.

B. On the azimuthal symmetry of the wake

It has been observed that any slight perturbation of the set-up leads to an asymmetric wake. The work of Mittal *et al.*¹¹ on shedding activity past spheres highlights that the Reynolds number impacts the azimuthal position of the oscillating global mode $m = 1$. It appears that after the unsteady bifurcation at $Re \approx 277$ over a sphere, the global mode has a preferred azimuthal orientation which may evolve at very low frequency. This effect disappears as Reynold number increases and the wake gets statistically axisymmetric in turbulent flows. In our experiments even at moderate Reynolds number, the wings prevent the statistical wake axisymmetry. The shedding occurs mostly at the upper and lower part of the wake corresponding respectively to topology #2 and #1 but the mean flow keeps the top-bottom symmetry.

Any non-axisymmetric disturbance leads to a preferred azimuthal orientation for the antisymmetric global mode. For example, as soon as the body has a small pitching angle, the shedding occurs exclusively at the upper part of the wake or lower part depending on the sign of ϵ and the wake loses this statistical symmetry. Therefore, if the disturbance has an azimuthal periodicity $m = 1$, the shedding occurs in the same azimuthal plane, at the same side or the opposite one depending on

the position of the perturbation. This point was proved by Meliga *et al.*²⁶ at low Reynolds numbers through a theoretical analysis. Over blunt bodies of revolution, the forcing term associated to the presence of a $m = 1$ disturbance selects the plane of symmetry of the first bifurcation. The different bifurcations observed in the wake of a disk degenerate into imperfect bifurcations and the flow remains tridimensional, its orientation based on the azimuthal position of the perturbation. When the disturbance has a higher azimuthal periodicity $m \geq 2$, for example the two wings in our experimental set-up associated to $m = 2$, the wake follows a statistical m flow topology. The main coherent structure remains a $m = 1$ global mode shifting randomly between the m preferred locations and generating a m statistical wake.

As a consequence, the experimental sensitivity analysis of the oscillating or helical mode $m = 1$ to an antisymmetric perturbation can only be studied in the azimuthal plane of the disturbance. The global mode follows any change of azimuthal position of the control leading to a mode sensitivity independent of the azimuth.

The planar symmetry being set, the azimuthal phase of the wake is then 0 or π referring to the position of the disturbance. The rate $d\delta_M^*/dx^*$ may play a dominant role for the selection of the phase, *i.e.* state #1 or #2. If one side of the axisymmetric mixing layer has a higher growth rate, as previously seen, the development of δ_M toward the recirculation bubble is enhanced. Thus, the curvature of the streamlines is increased²⁷ and the whole wake is shifted to the opposite side where the mixing layer remains thin. This concentration of vorticity leads to rolls-up and the development of the vortex loops presented by Sakamoto & Haniu¹⁰.

This analysis coincides with the effect of small pitching angles ϵ and positions of the control cylinder. Indeed over a nose-up configuration the upper boundary layer faces a higher adverse pressure gradient than the lower one. This results in an increased height and a higher turbulence level at the trailing edge. Therefore, the spread of the mixing layer is more intense on the upper side of the recirculation bubble and the wake moves down, the vortex loops being generated from the lower side of the bubble (see Fig. 5). In the same way, the control cylinder can enhance or reduce the rate $d\delta_M^*/dx^*$. In the close wake, when located in the inner part of the mixing layers the flow may reattach on it, inhibiting the shear layers instability. Then the opposite mixing layer grows faster and the wake moves in the direction of the disturbance (see Fig. 8(a)). Further downstream or in the outer mixing layers, the control cylinder has its own wake generating important fluctuations of the velocity fields. The disturbance intensifies the growth of the mixing layer and the wake moves to the other side. Only cylinder positions in the mixing layers in plane $z^* = 0$ are discussed

here ; when located inside the recirculation bubble, the cylinder get through the entire wake, the disturbance is then much more complicated. The presented interpretation is no more pertinent.

V. CONCLUDING REMARKS

In conclusion, the natural flow over a body with an axisymmetric detachment is proved to be a mean of asymmetric topologies. Due to the presence of two wings, *i.e.* $m = 2$ azimuthal periodicity of the body, the wake is not axisymmetric but keep a statistical $m = 2$ symmetry. Instantaneous wake follows a $m = 1$ azimuthal topology and is oriented either above or below the streamwise axis (phase 0 or π), shifting randomly. The unsteady global mode then develops from one side of the bubble depending on the orientation of the instantaneous wake.

A $m = 1$ disturbance, small pitching angle or control cylinder, sets one of the two asymmetric topologies depending on its characteristics. This study highlights that the sensitivity of the flow over a body of revolution to a non-axisymmetric local disturbance may only be observable in the azimuthal plane of the perturbation. Any shift in the azimuthal position of the disturbance will be followed by an equal shift of the azimuthal orientation of the global mode.

The use of control rings to generate a $m = 0$ disturbance has a strong influence on drag and wake. As observed by Meliga *et al.*⁶, the effect follows the position of the mixing layers of the natural flow. In particular, when placed in the inner part of the mixing layer, the rings may prevent the development of the shear layer instability. It reduces the global mode frequency and moves the wake structures downstream inducing significant drag reductions.

The mean flow symmetry as well as the global mode development are then highly sensitive to any disturbance in the recirculation area, particularly when the mixing layers equilibrium or characteristics are altered. The growth rate of the turbulent mixing layer seems to be a critical factor for the flow dynamics, more than the inviscid dynamics induced by the vorticity.

Eventually, these results might be associated to the disturbance of the reminiscent global modes observed in laminar regimes. The steady asymmetric wake reported after the first bifurcation may concentrate the sensitivity to $m \geq 1$ disturbances whereas the oscillating mode from the second bifurcation (oriented along the steady asymmetric mode) seems more sensitive to $m = 0$ perturbations.

Acknowledgements

The authors wish to thank P. Meliga for fruitful scientific discussions.

- ¹ D. Hill, A theoretical approach for analyzing the restabilization of wakes, NASA STI/Recon Technical Report N 92 (1992) 29394.
- ² O. Marquet, D. Sipp, L. Jacquin, Sensitivity analysis and passive control of cylinder flow, *Journal of Fluid Mechanics* 615 (-1) (2008) 221–252.
- ³ P. Luchini, F. Giannetti, J. Pralits, Structural sensitivity of the finite-amplitude vortex shedding behind a circular cylinder, in: *IUTAM Symposium on Unsteady Separated Flows and their Control*, Springer, 2009, pp. 151–160.
- ⁴ P. Strykowski, K. Sreenivasan, On the formation and suppression of vortex ‘shedding’ at low Reynolds numbers, *Journal of Fluid Mechanics* 218 (1990) 71–107.
- ⁵ P. Meliga, J. Chomaz, D. Sipp, Unsteadiness in the wake of disks and spheres: Instability, receptivity and control using direct and adjoint global stability analyses, *Journal of Fluids and Structures* 25 (4) (2009) 601–616.
- ⁶ P. Meliga, D. Sipp, J. Chomaz, Open-loop control of compressible afterbody flows using adjoint methods, *Physics of Fluids* 22 (2010) 054109.
- ⁷ H. Sakamoto, H. Haniu, K. Tan, An optimum suppression of fluid forces by controlling a shear layer separated from a square prism, *ASME Transactions Journal of Fluids Engineering* 113 (1991) 183–189.
- ⁸ V. Parezanović, O. Cadot, The impact of a local perturbation on global properties of a turbulent wake, *Physics of Fluids* 21 (2009) 071701.
- ⁹ V. Parezanović, O. Cadot, Experimental sensitivity analysis of the global properties of a 2D turbulent wake, *Journal of Fluid Mechanics* accepted for publication.
- ¹⁰ H. Sakamoto, H. Haniu, A study on vortex shedding from spheres in a uniform flow, *ASME, Transactions, Journal of Fluids Engineering* 112 (1990) 386–392.
- ¹¹ R. Mittal, J. Wilson, F. Najjar, Symmetry properties of the transitional sphere wake, *AIAA journal* 40 (3) (2002) 579–582.
- ¹² S. Taneda, Visual observations of the flow past a sphere at Reynolds numbers between 104 and 106, *Journal of Fluid Mechanics* 85 (01) (1978) 187–192.
- ¹³ H. Pao, T. Kao, Vortex structure in the wake of a sphere, *Physics of Fluids* 20 (1977) 187.
- ¹⁴ E. Berger, D. Scholz, M. Schumm, Coherent vortex structures in the wake of a sphere and a circular disk at rest and under forced vibrations, *Journal of Fluids and Structures* 4 (3) (1990) 231–257.
- ¹⁵ G. Yun, D. Kim, H. Choi, Vortical structures behind a sphere at subcritical Reynolds numbers, *Physics of Fluids* 18 (2006) 015102.

- ¹⁶ W. Mair, The effect of a rear-mounted disc on the drag of a blunt-based body of revolution(Drag of body of revolution with blunt base substantially reduced by mounting disk behind body with smaller diameter than body), *Aeronautical Quarterly* 16 (1965) 350–360.
- ¹⁷ A. Weickgenannt, P. Monkewitz, Control of vortex shedding in an axisymmetric bluff body wake, *European Journal of Mechanics-B/Fluids* 19 (5) (2000) 789–812.
- ¹⁸ A. Sevilla, C. Martinez-Bazan, Vortex shedding in high reynolds number axisymmetric bluff-body wakes: Local linear instability and global bleed control, *Physics of Fluids* 16 (2004) 3460.
- ¹⁹ H. Higuchi, Passive and Active Controls of Three-Dimensional Wake of Bluff-Body, *JSME International Journal Series B* 48 (2) (2005) 322–327.
- ²⁰ J. Morrison, A. Qubain, Control of an axisymmetric turbulent wake by a pulsed jet, *Advances in Turbulence XII* (2009) 225–228.
- ²¹ F. Champagne, Y. Pao, I. Wygnanski, On the two-dimensional mixing region, *Journal of Fluid Mechanics* 74 (02) (1976) 209–250.
- ²² H. Schlichting, K. Gersten, K. Gersten, *Boundary-layer theory*, Springer Verlag, 2000.
- ²³ J. Delery, Topologie des écoulements tridimensionnels décollés stationnaires : points singuliers, séparatrices et structures tourbillonnaires, Tech. rep., RT 121/7078 DAFE/N. ONERA (1999).
- ²⁴ E. Achenbach, Vortex shedding from spheres, *Journal of Fluid Mechanics* 62 (02) (1974) 209–221.
- ²⁵ J. Gerrard, The mechanics of the formation region of vortices behind bluff bodies, *Journal of Fluid Mechanics* 25 (02) (1966) 401–413.
- ²⁶ P. Meliga, J. Chomaz, D. Sipp, Global mode interaction and pattern selection in the wake of a disk: a weakly nonlinear expansion, *Journal of Fluid Mechanics* 633 (-1) (2009) 159–189.
- ²⁷ R. Simpson, Turbulent boundary-layer separation, *Annual Review of Fluid Mechanics* 21 (1) (1989) 205–232.